Sub-50 fs temporal resolution in an FEL-Optical laser pump-probe experiment at FLASH2

ATIA-TUL-NOOR[1,*,§], SONU KUMAR[1,§], NORA SCHIRMEL[1], BENJAMIN ERK [1], BASTIAN MANSCHWETUS[1,2], SKIRMANTAS ALISAUKAS[1], MARKUS BRAUNE[1],GIOVANNI CIRMI[1], MARIE KRISTIN CZWALINNA[1], ULRIKE FRÜHLING[1], UWE GROSSE-WORTMANN[1],NICK KSCHUEV[1], FREDERIK KUSCHEWSKI[1,3], TINO LANG[1], HANNES LINDENBLATT[4], IGOR LITVINYUK[5], SEVERIN MEISTER[4], ROBERT MOSHAMMER[4], CHRISTINA C. PAPADOPOULOU[1], CHRISTOPHER PASSOW[1], JULIANE ROENSCH-SCHULENBURG[1], FLORIAN TROST[4],INGMAR HARTL[1], STEFAN DÜSTERER[1], SEBASTIAN SCHULZ[1,†]

[1] *Deutsches Elektronen-Synchrotron DESY, Notkestr. 85, 22607 Hamburg, Germany*
[2] *currently with Class 5 Photonics, Notkestr. 85, 22607 Hamburg, Germany*
[3] *currently with German Aerospace Centre, Institute of Quantum Technologies 89081 Ulm, Germany*
[4] *Max-Planck-Institut für Kernphysik, Saupfercheckweg 1, 69117 Heidelberg, Germany*
[5] *Centre for Quantum Dynamics and Australian Attosecond Science Facility, Griffith University, Science Rd., Nathan, QLD, 4111, Australia*
[§] *The authors contributed equally to this work.*
[*] *atia.tul.noor@desy.de*
[†] *sebastian.schulz@desy.de*

Abstract: High temporal resolution is essential for ultra-fast pump-probe experiments. Arrival time jitter and drift measurements, as well as their control, become critical especially when combining XUV or X-ray free-electron lasers (FELs) with optical lasers due to the large scale of such facilities and their distinct pulse generation processes. This paper presents the application of a laser pulse arrival time monitor that actively corrects the arrival time of an optical laser relative to the FEL's main optical clock. Combined with post-analysis single pulse jitter correction this new approach improves the temporal resolution for pump-probe experiments significantly. Benchmark measurements on photo-ionization of xenon atoms performed at beamline FL26, FLASH in Hamburg, Germany, demonstrate a sub-50 fs FWHM overall temporal resolution.

1. Introduction

Real-time imaging of ultra-fast phenomena on the femtosecond timescale became feasible with recent developments in technology and the application of novel methodologies. Femtosecond pump-probe spectroscopy is nowadays a commonly used technique that has increased our understanding of fundamental photo-induced dynamical processes in physics, chemistry, and biology [1]. Two ultra-short light pulses are employed to investigate the dynamical properties of a system, where one laser pulse is used to initiate ("pump") a certain reaction, and the delayed second pulse is used to measure ("probe") the dynamics introduced by the first pulse. This allows, for example, the mapping of a photo-chemical reaction on timescales of picoseconds down to attoseconds. Such timescales are native to the electronic processes that track the evolving geometric structures of a molecule undergoing a reaction. To effectively interpret any study on ultra-fast dynamics, it becomes imperative to achieve high temporal resolution, which relies on the precise characterization of the pulse durations as well as the exact knowledge of the delay between the pulses.

Combining intense, short pulse near-infrared (NIR) lasers and free-electron laser (FEL) sources has enabled new ways to obtain insight into photo-induced processes and their evolution often utilizing the site specificity of the high energy FEL interaction (see e.g. [2–4]). Several such pump-probe experiments have already been performed at the high repetition rate XUV and soft X-ray Free-electron LASer in Hamburg (FLASH) in recent years, with notable examples being discussed in e.g. [5–16].

In pump-probe experiments using conventional ultra-fast laser technology, both pump and probe beams are typically generated from a common laser source. Even in this case, the transportation of these beams from the laser to the experiment is susceptible to disturbances due to fast relative timing jitters and slow timing drifts caused by acoustical vibrations, pointing fluctuations, and environmental changes on a day-to-day basis. Typically, these laser systems, including the beam transport to the pump-probe setup are relatively compact (a few meters). Whereas at a large-scale facility such as FLASH, for ultra-fast pump-probe experiments, an optical femtosecond laser needs to be exactly timed with precise delay and low jitter with the intense extreme ultraviolet (XUV) or X-ray pulses from an about 300 m long accelerator-based source [17]. In this case, the long-distance transport via non-common beam paths and its sensitivity to different environmental factors like humidity, pressure, temperature, vibrations, and airflow, make it technically challenging to establish robust and drift-free temporal stability between the pump and probe pulses. Particularly, typical data acquisition times can vary between a few hours and several days, thus stable temporal conditions in the experiment become even more crucial. Without further measures, the relative drift in arrival time between optical laser and FEL pump-probe pulses within the time span of a typical pump-probe experiment can exceed hundreds of femtoseconds. The origin of those timing drifts can be caused by factors such as fluctuations in the electron beam acceleration, or the timing stability of the optical laser, both with respect to a timing reference. To establish a facility-wide timing stabilization on the femtosecond level, at FLASH all critical subsystems are individually stabilized with respect to the same optical reference clock [17]. Several approaches have been implemented for the accurate control of the timing between both sources with appropriate diagnostics at different FEL facilities around the world. For example, the European XFEL (EuXFEL) achieved in a short pulse operation mode sub-20 fs precision in a recent soft X-ray photo-electron spectroscopy experiment [18], whereas at the Linac Coherent Light Source (LCLS) temporal resolution in the ∼30 fs range has been demonstrated [19], while the typical optical laser/X-ray pump-probe experiment temporal resolution is in the range of 60 fs (FWHM) [20]. FERMI [21] an externally seeded FEL facility, provides X-ray pulses with extremely small timing jitter (sub-5 fs) [22] with respect to the optical laser. Still, the temporal resolution is in the range of 100 fs (FWHM) [23,24] limited by the optical pulse duration rather than jitter or drift. It is important to recognize that temporal resolution can vary strongly based on parameters and specific settings used in each study. Despite advanced timing schemes, the typical temporal resolution achieved in two-color pump-probe experiments performed at the FLASH2 FEL beamline of FLASH, so far, is in the range of 150-300 fs, significantly larger than expected from the contributing pulse durations alone [6–9].

In this work, we study the different components of timing stabilization and the overall temporal resolution currently achievable at the FLASH2 beamline FL26. An optical Laser pulse Arrival time Monitor (LAM) has been implemented for drift compensation in an active feedback loop. Additionally, we incorporate the single pulse correction method according to the electron bunch arrival time data in post-analysis for fast fluctuations. Employed in a time-resolved experiment, drift compensation and jitter correction can dramatically improve the temporal resolution to below 50 fs (FWHM) in a benchmark measurement for the case of xenon photo-ionization.

2. Experimental Setup

FLASH [25, 26] is a 315 m long FEL facility at DESY, Hamburg, Germany, operating with the Self-Amplified Spontaneous Emission (SASE) principle, delivering intense femtosecond pulses in the XUV and soft X-ray energy range. The pulse duration can be varied in the range of sub 10 fs to several 100 fs [25, 27, 28]. FLASH2 [29] is the second FEL beamline of FLASH, which can generate pulses in a wide spectral range from 14 eV to about 360 eV in the fundamental and about 1 keV in the 3rd harmonic, featuring variable-gap undulators that offer (limited) continuous wavelength tunability for fixed accelerator settings. FLASH operates in a burst-mode pulse pattern, where at 10 Hz bursts of up to 800 pulses can be produced with an intra-burst repetition rate of up to 1 MHz. This peculiar pattern poses challenging boundary conditions for detectors and optical lasers following the identical pattern. A wavelength-tunable pump-probe NIR laser based on optical parametric chirped-pulse amplification (OPCPA), that can resemble this burst mode, is available and can be delivered to the FLASH2 photon beamline end-stations [30, 31]. The experiment presented in this work was performed at the reaction microscope (REMI) [32, 33] end-station at the photon beamline FL26 [34]. At this instrument, the combination of high repetition-rate XUV-FEL and NIR-laser pulses together with coincidence detection schemes for ionic fragments and electrons enables XUV-NIR pump-probe experiments to investigate ultra-fast phenomena in gas-phase systems.

2.1. The FLASH timing system

A simplified schematic overview of the FLASH facility with a particular focus on the FLASH2 experimental hall with its photon beamlines is shown in Fig. 1. A comprehensive description can be found in refs. [25, 26]. The electron bunches (moving from left to right in Fig. 1), created at the electron gun, are accelerated to relativistic energies by passing through several superconducting accelerator modules, before entering the undulators where FEL radiation is produced by the SASE process. The FEL radiation is transported to the experimental hall through photon beamlines, including a photon diagnostics section, and distributed to different beamlines and experimental end-stations by switchable mirrors.

Along the accelerator, several beam arrival monitors (BAM) are installed for arrival time measurements of the electron bunches. This arrival-time data is used as an error signal in longitudinal stabilization feedback systems which stabilizes the arrival time of the electron bunches along the bunch train at several sections and ultimately the arrival time of the photon pulses. Details can be found in [35, 36]. To ensure precise timing among all relevant subsystems of FLASH, the main oscillator (MO) provides radio frequency (RF) reference signals throughout the facility. For those subsystems that need the highest timing stability (e.g. BAMs and external pump-probe laser systems) a main laser oscillator (MLO), which itself is synchronized to the RF oscillator reference, provides ∼200 fs long pulses at 1550 nm and 217 MHz as a highly stable optical reference. The MLO pulses are distributed through optical path length stabilized optical fibers, shown schematically in Fig. 1 as dark blue arrows, resulting in their arrival time being stabilized to the 1 fs level using balanced optical cross-correlators (BCCs) [37, 38]. One of the BCCs (BCC 1 in Fig. 1) is used in the precision timing of the seed laser oscillator (∼170 fs, 1030 nm, 54 MHz) of the FLASH2 pump-probe laser system to the MLO reference, resulting in a remaining jitter which can be as low as 5±1 fs rms [17] by activating the feedback loop (FB 1), which acts on the oscillator cavity length. To precisely control the delay between the optical timing reference and the FLASH2 laser oscillator, a mechanical delay stage (Delay 1) is used in the reference's beam path. This essentially can be used to control the time delay between NIR laser and FEL pulses. The pulses of the pump-probe laser oscillator are subsequently amplified by several Ytterbium-based fiber pre-amplifiers as well as a high-power chirped-pulse solid-state amplifier system (CPA). A multi-stage optical parametric amplification system (OPCPA) is pumped by the second harmonic CPA system and seeded by a super-continuum source driven

by the common fiber pre-amplifier. The OPCPA provides wavelength-tunable high-power laser pulses supporting pulse duration shorter than 15 fs. Since the pump-probe laser system is located in an environmentally stabilized hutch (Laser Lab) within the FLASH experimental hall, the laser beam is relay imaged through an approximately 40 meters long, evacuated transport beamline to a laser table (MOD2.6) next to the REMI instrument. There, the laser pulses are compressed and propagated more than 10 meters in the air within the optical setup on the laser table before they are coupled into the vacuum chamber of the REMI.

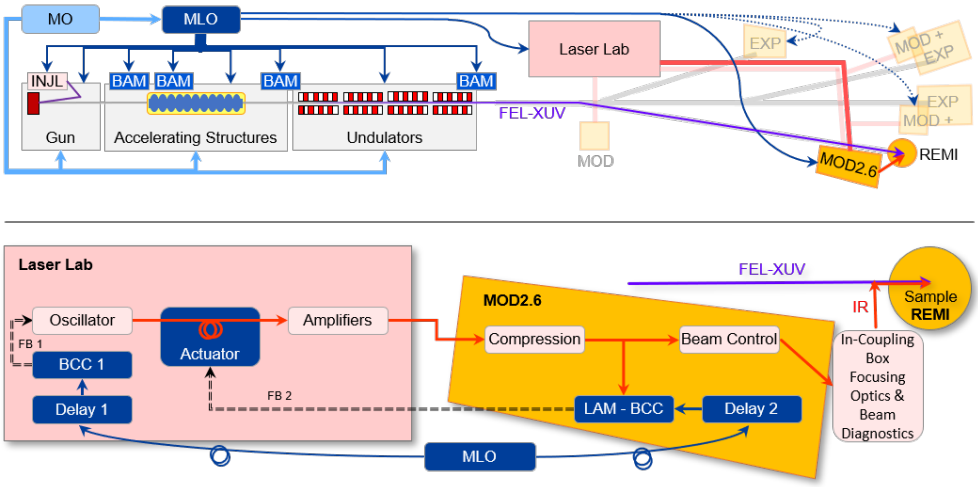

Fig. 1. A schematic layout of the FLASH facility and FLASH2 experimental hall, Laser lab in pink, and laser safety hutch in yellow (bottom part zoomed in pink and yellow) including some important elements of the timing and diagnostics system. The electron bunches are generated at the so-called "gun" by the photo-injector laser (INJL) and are accelerated with superconducting accelerator modules up to a maximum of 1.35 GeV. The radio frequency (RF) main oscillator (MO) provides the reference signals for the gun and the accelerator of FLASH, as well as the MLO. BAMs are installed in timing critical sections of the linear accelerator and at the end of the undulators to measure and provide feedback to stabilize the relative timing of electron bunches with respect to the MLO. The BCCs are a central part of the synchronization. They are used to synchronize the pump-probe laser to the MLO and, in particular, the LAM is also based on a BCC and can be used to compensate drifts arising in the laser amplification and transport. The pump-probe laser system is located in the laser lab in the experimental hall. The experiment is carried out at the REMI end-station by combining the FEL pulses (in purple) with a synchronized pump-probe laser (in red) that is delivered via ~40 m long evacuated tubes (top part, red lines) towards the laser table located in a laser safety enclosure MOD2.6 next to the experimental chamber.

2.2. The laser arrival time monitor and active feedback for drift compensation

The overall drifts in the optical path length of the pump-probe laser pulses are mainly caused by the remaining temperature and humidity changes in the laser lab, as well as the temperature-dependent geometrical path length of the long-distance vacuum beam transport and the optical setup directly at the end-stations exposed to the experimental hall of FLASH2. It should be noted that temperature and humidity conditions at the end-stations are with typical fluctuations of ±1 K and ±30% RH respectively. These fluctuations are considerably less favorable for passive stability of the optical beam path length than in the laser lab itself which experiences typically ±0.1 K and ±5 %RH.

To compensate for arrival time drifts, the laser is equipped with slow drift compensation feedback (FB 2). A temperature-controlled fiber coil, which consists of ~30 m temperature-stabilized fiber and ~5 m actively temperature-controlled polarization maintaining (PM) single mode fiber, serves as a feedback actuator. It allows for control of the arrival time by continuous temperature adjustment with a coefficient of 330 fs/K within a total range of 8.9 ps.

To quantify and compensate drifts occurring in the laser system as well as in the beam transport and on the laser table next to the experiment, the LAM, which originally had been developed for the synchronization of laser oscillators within the laser-based synchronization system at FLASH [17], was installed as close as possible to the experimental end-station. It consists of a BCC (LAM-BCC in Fig. 1) and a motorized translational delay stage (Delay 2). The LAM is located in the laser safety enclosure of the FL26 end-station, called Modular Optical Delivery Station (MOD2.6), shown schematically in Fig. 1. In Fig. 2 an overview of the laser beam propagation and the LAM setup inside MOD2.6 is presented. After pulse compression, a fraction of the laser pulse energy is sent to the LAM-BCC, while the main part is sent to the experimental end-station. In the LAM-BCC the temporal overlap between the reference from MLO and NIR pulses is adjusted with Delay 2. The detailed working principle can be found in [17, 37, 38].

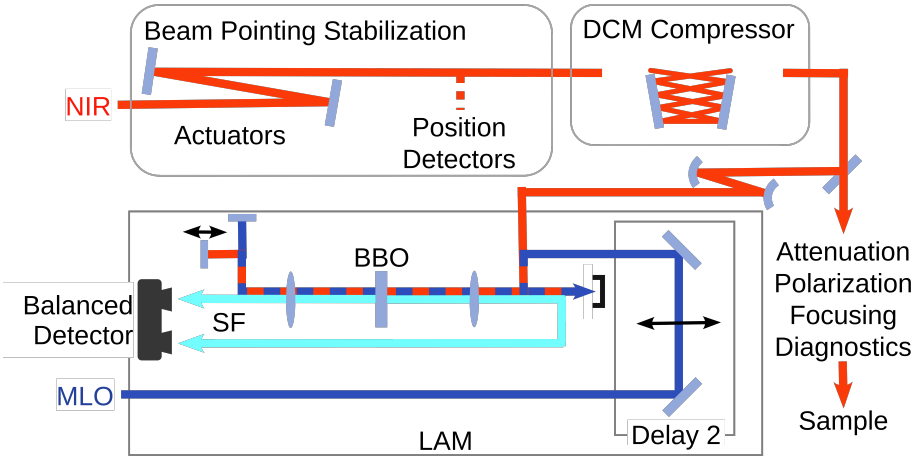

Fig. 2. Schematic laser setup of MOD2.6. After leaving the vacuum beam transport pipe the NIR laser (in red) is pointing stabilized and the pulses are compressed in a double chirped mirror (DCM) compressor. Afterward, a sampled beam is sent to the LAM while the main beam passes controls and diagnostics, and propagates to the experimental end-station. In the LAM the laser pulses are combined with the MLO reference (in blue) and focused into a BBO crystal for sum frequency generation (SF, in cyan). The temporal overlap between laser and reference pulses is adjusted with Delay 2 in the reference beam path. After passing the BBO once, the laser is slightly delayed with respect to the reference and both, the laser and reference, are sent back for a second pass through the crystal. The SF signals from both passes are detected in a balanced photodiode detector, from which the error signal for FB 2 is generated.

The error signal from the LAM can now be used in an active feedback loop (FB 2 in Fig. 1) to compensate for and eliminate timing drifts and slow timing fluctuations. According to the LAM error signal, the laser arrival time can be stabilized by adjusting the path length between the oscillator and the laser amplifier through FB 2 with the temperature-controlled fiber coil. FEL-laser pump-probe experiments require of course not only a well-stabilized but also precisely scannable arrival time of the laser pulses with respect to the FEL pulses. Therefore, the laser pulse arrival time can be controlled by delaying the LAM reference with delay stage 2 and relying on FB 2 to shift the arrival time of the pump-probe laser accordingly through fiber temperature

adjustments.

Figure 3a illustrates the performance of the feedback over 12 hours of measurement. It consists of multiple data sets where the pump-probe delay is scanned over a duration of approximately 7 hours. The gaps observed in Fig. 3a result of the interruption and resumption of the data acquisition. The first experimental run spans over a period of ∼4 hours. The pump-probe laser parameters for the data presented in Fig. 3(a,b) were 18 fs (FWHM) pulse duration after compression at 800 nm center wavelength with bursts of 70 pulses and 100 kHz intra-burst repetition rate. Data was recorded with a 10 Hz repetition rate and the arrival time measured by the LAM was averaged over all pulses in each burst. The result of the actively stabilized arrival time using feedback FB 2 is shown in green and yellow. The feedback controls the temperature of the fiber coil in FB 2 in order to minimize the error signal of the LAM, which is a measure of the relative time delay in femtoseconds between the MLO fiber link and pump-probe laser pulses. With the feedback active, the arrival time stability is determined to be ∼10 fs rms, and the drifts averaged over five minutes are substantially reduced to less than 1 fs rms (shown in yellow). To visualize the expected drift of the laser arrival time without FB 2, the compensated drifts can be calculated back from the fiber temperature change of the fiber actuator ("corrected drift" in blue). This visualization shows large drifts within a time frame of 12 hours, with a peak-to-peak drift of approximately 500 fs and a residual jitter of 21 fs rms when subtracting a five-minute rolling average (shown in red). The active feedback therefore not only increases the achievable time resolution significantly, but it crucially eliminates the need for additional experimental strategies such as frequent interruptions to measure and adjust the temporal overlap between FEL and NIR laser. This, in turn, leads to the much easier analysis of the acquired data as the temporal overlap between FEL and NIR is kept stable within ±30 fs (comparing different runs taken over two days not shown here).

The effect of a delay scan on the relative arrival time over a duration of ∼4 hours for one experimental run, marked in 3a, is presented in Fig. 3b. Delay 2 is used to shift the timing reference signal for the LAM (black) which is then immediately followed by adjustment of the pump-probe laser arrival time through FB 2 (red), the difference between black and red is due to the simultaneous compensation of the drifts by the feedback. The delay was scanned over a range of 1 ps with a step size of 30 fs. Since FB 2 acts without significant time delay, as expected, no significant influence from the delay scan can be observed in the LAM in-loop jitter and drift measurement as shown in Fig. 3a. The pump-probe laser arrival time follows the timing reference for the LAM and thus is well defined over ≈4 hours delay scan. It can be concluded that FB 2 and temperature-controlled fiber coil are fully capable of being used not only for drift stabilization but also for delay scans of standard user experiments which typically operate within the above-presented boundary conditions, with many experiments scanning much slower and over smaller ranges.

3. Xenon experimental results as a benchmark for the achieved time-resolution

To demonstrate the performance of the active LAM feedback and data sorting in post-analysis, an atomic physics XUV-optical pump-probe experiment has been carried out.

The experiment was performed at the reaction microscope (REMI) end-station at beamline FL26 at FLASH2 [34]. The REMI instrument is designed for measuring the three-dimensional momenta of ions and electrons in coincidence from low-density gas-phase samples to investigate atomic, molecular, and optical (AMO) physics. For the presented data, the FLASH accelerator was tuned to an electron energy of 925 MeV. The generated XUV pulses show a central wavelength of 7.7 nm and a broad pulse energy distribution with an average of 2.5 µJ in the interaction region. The pulse duration of the XUV pulses is estimated to (20 ± 10) fs FWHM (thus, containing only a few temporal modes) based on the analysis of the statistical fluctuation of the XUV pulse energy [39–41] and the used accelerator settings [27]. The data acquisition system (DAQ) at

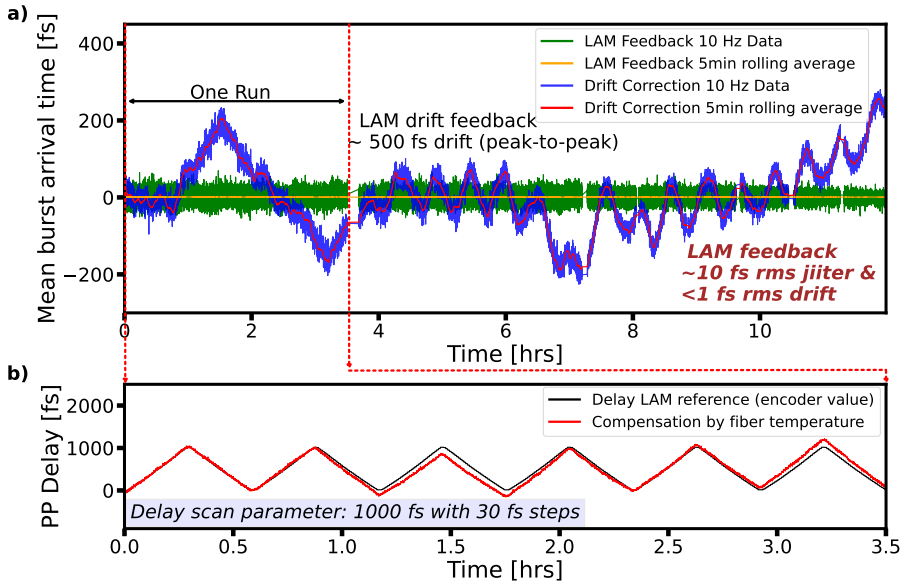

Fig. 3. a) In-loop drift measurement of the LAM with internal feedback FB 2 over 12 hours. The mean values of the arrival time over a burst, recorded with a repetition rate of 10 Hz, are represented in green whereas the yellow line is the five-minute rolling average. Data in blue is the compensated drift back-calculated by converting the applied fiber temperature change into time. This shows a drift of ~ 500 fs peak-to-peak drift and variations over 12 hours. b) Measured delay stage position (black) followed by fiber temperature (red) over ~ 4 hours of laser operation marked as "one run" in panel a) is shown. The scan range is 1 ps with a 30 fs step size. The arrival time of the laser pulse is scanned by delaying the LAM reference through FB 2 which in turn shifts the arrival time of the pump-probe laser achieved by fiber temperature adjustments (shown in red).

FLASH records a large number of parameters for each pulse, such as the XUV and NIR laser pulse energy, the electron bunch and laser pulse arrival times, delay stage positions, and the fiber-coil temperature. These parameters can be used in the post-analysis to sort and correct the measurement data [7, 42].

The pump-probe laser pulses pass through the beam control and diagnostics section after the compressor stage (see Fig. 2). It consists of several glass plates of variable thickness to control and measure the laser pulse duration and a mirror-based focusing telescope. The NIR beam is coupled into the vacuum through a 3.5 mm thick BK7 window and reflected by a mirror under 45 deg, which has a centered, 4 mm diameter hole for the FEL to pass through. The NIR laser has a central wavelength of 800 nm and a pulse duration of 18 fs (FWHM), a pulse energy of 110 µJ, and a focal spot size of 50 µm. FEL and optical laser are operated at 10 Hz burst mode with 100 kHz intra-burst repetition rate and 50 pulses per burst. The sample is introduced via supersonic expansion in a continuous gas jet [34]. This gas beam propagates perpendicular to the XUV and laser beams, crossing them in the interaction region at the center of the REMI main chamber. The generated ions are extracted by a homogeneous electric field and are directed onto a time and position-sensitive detector.

The laser-assisted x-ray photo-ionization in Xe atoms [43] can be used to quantify the temporal resolution of a pump-probe experiment. The photons of ~160 eV photon-energy from the

FEL pump-pulse are used to ionize the Xe atoms from the 4d and 4p shell leaving a core-hole behind. This hole is filled within femtoseconds via an Auger-Meitner decay, producing Xe^{2+} in the configuration of $5p^{-2}$ and also leading to high charge states involving several intermediate states [44]. Some of the intermediate states (namely $5s^{-1}5p^{-2}$6p as well as $5p^{-3}nl$ configuration) lie below the threshold for Xe^{3+} and a small fraction of Xe^{2+} population ending up in $5p^{-4}nln'l'$ configuration [45]. The NIR probe pulse arriving after the FEL pulse can efficiently ionize these excited intermediate states, inducing a delay-dependent rise in higher charge states and consequently a depletion of the Xe^{2+} ion yield. The lifetime of these states varies from a few fs to 100 ps [45, 46].

Figure 4 shows the Xe^{2+} ion yield as a function of XUV-NIR delay. For positive delays Xe^{2+}

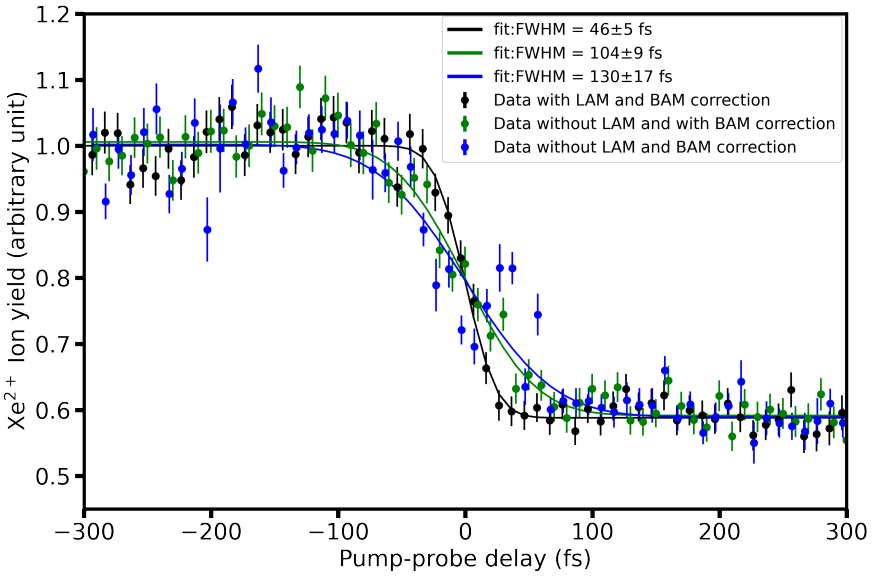

Fig. 4. The ion yields of Xe^{2+} versus delay between the XUV pump and the NIR probe. The data consists of a one-hour delay scan. At each delay setting, signals were accumulated for 30 seconds. The circles and the error bar show the average time re-binned data set using 10 fs time bins and the standard errors of the mean for this measurement. The curves are fitted with a step function (shown in blue, green, and black lines) convoluted with a Gaussian to model the pulse length and timing jitter broadening. The data set in blue relies on the intrinsic timing stability at FLASH2 including the slow drift without FB 2 (for visualization as discussed in section 2.2) resulting in a width of 131 fs FWHM. The green data set is the same as the blue with the addition of jitter correction for fast electron bunch arrival time fluctuations measured by the BAM. The width is reduced to 104 fs FWHM. In the black data set in addition the LAM feedback (FB 2) is actively compensating for slow drifts, reducing the width to 46 fs FWHM.

is predominantly in the ground state configuration $5p^{-2}$. For this measurement, the delay stage was scanned multiple times bidirectional over a range of ±0.5 ps. For an approximately one-hour delay scan, the delay stage position is changed in 30 fs step size and data was accumulated for 30 seconds at each delay position. In post-analysis data is sorted according to the pulse-to-pulse BAM values. To visualize the drift compensated by the LAM feedback, the drift calculated from

the fiber temperature change (discussed in section 2.2) is also included in the data frame. These values are subtracted from the delay-stage values and new delay values are binned such that each bin is normalized according to number of pulses and averaged into 10 fs wide bins. Negative time delays correspond to the arrival of the XUV pulse after the optical laser pulse. The normalization and jitter correction steps are described in detail in refs. [7, 42].

A Gaussian cumulative distribution function is used to fit the data to determine the zero temporal response time.

$$f(t) = a + b(erf(\frac{t - t_o}{\sigma})) \tag{1}$$

Here a and b are the base and amplitude, $erf()$ is the Gaussian error function, t_o is the center position of the step function and σ defines the rms width of the Gaussian error function. The width of the fitted error function is a convolution of the temporal profiles of the XUV, NIR pulses as well as residual temporal jitter and drifts. The fitted data, indicated in blue in Fig. 4 is without any correction and includes the drift that would have happened without the LAM feedback compensation (calculated from the feedback response i.e. fiber temperature change in actuator). The FWHM is approximately (131 ± 17) fs. The data, still without active LAM feedback FB 2, but including the fast jitter correction from pulse-to-pulse information recorded by the BAM, is shown in green, resulting in an enhanced (104 ± 9) fs FWHM signal width. The extracted temporal width for the data with active LAM feedback and pulse-to-pulse corrected for electron bunch arrival time is shown as the black line in Fig. 4. The active LAM feedback improves the time-resolution by a factor of two, leading to a temporal resolution of (46±5) fs FWHM.

To gain insight into the overall improved temporal resolution and to investigate its limitations, we discuss the known sources of jitters and drifts. Jitter is defined as the short-term temporal fluctuation of the arrival time on a pulse-to-pulse basis while the drift is defined over a longer time of minutes and hours. By taking the average of the data from pulse train, we can distinguish between long-term drifts and the jitter observed in individual pulses. The electron bunch arrival times are measured on pulse-to-pulse basis by the BAM and the resulting jitter with respect to MLO can be corrected with remaining uncertainty of the BAM resolution of σ_{BAM} about 5 fs rms (determined by the noise level of the measurement). The jitter contribution induced by SASE inherent arrival time fluctuations for 7 nm wavelength can be estimated to $\sigma_{SASE} \approx$3 fs rms [47].

The most significant factor that lowers the time resolution is the variability in the arrival time of the optical laser pulses. Here, drifts are spanning over hundreds of femtoseconds on the timescale of minutes and hours, as shown in Fig. 3a. The new, active LAM feedback corrects this slow drift within the laser transport system and compensates drifts from 500 fs peak-to-peak to $\sim$ 1 fs peak-to-peak. For pulse-to-pulse fluctuations, the LAM data evaluation shows a jitter $\sim$ 10 fs rms, which is comparable to the residual jitter of the laser oscillator with respect to the optical reference $\sigma_{Osc-MLO}$ of 6 fs rms. This indicates that the whole laser amplification and transport does mainly add slow arrival time drift, and negligible contributions to the overall timing jitter. Finally, the MLO and its optical distribution contribute with a very small jitter of only σ_{OptRef} $\sim$1 fs rms [17]. Thus, the total estimated jitter after sorting the data according to BAM can be approximated as

$$\sigma_{jitter} = \sqrt{(\sigma^2_{OptRef} + \sigma^2_{BAM} + \sigma^2_{SASE} + \sigma^2_{LAM-jitter})} \tag{2}$$

resulting in a total estimated jitter ~29 fs FWHM or ~12 fs rms.

The final experimental temporal resolution can be calculated by combining the calculated total jitter with XUV pulse duration ~(20±10) fs FWHM and NIR pulse duration ~(18±10) fs FWHM according to

$$\tau_{resolution} = \sqrt{(\tau^2_{XUV} + \tau^2_{Laser} + \sigma^2_{jitter})} \tag{3}$$

resulting in (40 ± 12) fs FWHM, which is within experimental uncertainty and in good agreement with the measured values.

Potential sources for the remaining drifts and jitter could be the components of the pump-probe laser system that were not included in the feedback, i.e. ≈4 meter of the NIR beam-path from the compressor inside the laser delivery setup at MOD2.6 (see Fig. 2) to the interaction region, as well as mechanical vibrations of optical components to the experimental end-station, which can be caused for instance by vacuum pumps. The length change of the remaining 4 m of the beam path is monitored during the experiment by an interferometer (SIOS SP 15000 NG, SIOS Messtechnik GmbH) with sub nm precision. The additionally introduced jitter was less than 1 fs rms and drift during the presented measurement was only 6 fs peak-to-peak. These factors are currently under investigation and measures are being evaluated, to mitigate such effects. Installing the LAM system closer to the experimental end-station as well as keeping the optical setup mechanically more stable will help to reduce the timing instability even further. Moreover, improvement in temporal resolution can be made by correcting and tracking the SASE-related instabilities and pulse-to-pulse laser arrival time also taking the environmental factors such as temperature, air pressure, and relative humidity on the optical laser path into account.

4. Conclusion and future outlook

In summary, we have implemented an active stabilization of the laser pulse arrival time by drift correction for the first time at the FLASH2 beamline FL26 and analyzed its performance. We have shown a benchmark pump-probe experiment, with ≈ 1 hour measurement time, on xenon photo-ionization with a temporal resolution of (46 ± 5) fs FWHM by additionally employing the single-pulse information of the electron beam arrival times. The observed improvement in time-resolution is significant, as before the implementation of these techniques, time-resolutions at this beamline typically were within the range of (150-300) fs FWHM.

This improved time resolution significantly extends the experimental capabilities of the FLASH facility and enables the study such as vibrations, charge migration [48] and lifetime of transient excited states [45] in small to intermediate molecules which were not possible with such a good temporal resolution in a two-color pump-probe experiment before at FLASH. The ability to investigate these processes in real-time offers significant advantages over traditional spectroscopic methods, which typically provide information averaged over longer time intervals. Furthermore, feedback keeps the temporal overlap constant with a precision of ± 30 fs and allows for more efficient data acquisition without the need for overlap checks.

Controlling the environmental factors and keeping the detectors for the feedback system as close as possible to the experimental end-station can substantially enhance the timing stability. Further upgrades and improvements to measure the timing jitter are under consideration in order to enable pump-probe experiments with a timing resolution in the order of 10 fs or below.

Acknowledgments. We acknowledge DESY (Hamburg, Germany), a member of the Helmholtz Association HGF, for the provision of experimental facilities. Parts of this research were carried out at FLASH2, REMI end-station at beamline FL26 and we would like to thank machine operators, run coordinators, laser and synchronization team for assistance. The data was taken in the beamtime ID 11015327.

Disclosures. The authors declare no conflicts of interest.

Data Availability Statement. Data underlying the results presented in this paper are not publicly available at this time but may be obtained from the authors upon reasonable request.

Author contributions. A.T.N, S.K, C.P processed the Xenon experimental data, performed the analysis. A.T.N, S.K, N.S drafted the manuscript and designed the figures with contributions from all authors. U.F, C.P, I.L, H.L, F.T, S.M, C.C.P, A.T.N, S.K, B.M, B.E performed the xenon measurement at the REMI end-station. T. L, S.A, G.C, S.K, N.S, B.M set up the laser parameters. S.S and N.K implemented the reference optical main laser oscillator. S.S, N.K, N.S, F.K and U.G setup the LAM feedback. J.R, M. K. C,

S.D implemented the beam-based accelerator stabilization and short XUV pulses. S.D., S.K, and B.E set up the SIOS interferometer. All authors contributed to the discussion.

References

1. A. H. Zewail, "Femtochemistry: Atomic-scale dynamics of the chemical bond," The J. Phys. Chem. A **104**, 5660–5694 (2000).
2. J. Rossbach, J. R. Schneider, and W. Wurth, "10 years of pioneering x-ray science at the free-electron laser flash at desy," Phys. Reports **808**, 1–74 (2019).
3. D. Rolles, "Time-resolved experiments on gas-phase atoms and molecules with xuv and x-ray free-electron lasers," Adv. Physics: X **8**, 2132182 (2023).
4. C. Bostedt, S. Boutet, D. M. Fritz *et al.*, "Linac coherent light source: The first five years," Rev. Mod. Phys. **88**, 015007 (2016).
5. K. Schnorr, A. Senftleben, G. Schmid *et al.*, "Multiple ionization and fragmentation dynamics of molecular iodine studied in ir–xuv pump–probe experiments," Faraday Discuss. **171**, 41–56 (2014).
6. F. Lever, D. Mayer, D. Picconi *et al.*, "Ultrafast dynamics of 2-thiouracil investigated by time-resolved auger spectroscopy," J. Phys. B: At. Mol. Opt. Phys. **54**, 014002 (2020).
7. D. Mayer, F. Lever, and M. Gühr, "Data analysis procedures for time-resolved x-ray photoelectron spectroscopy at a sase free-electron-laser," J. Phys. B: At. Mol. Opt. Phys. **55**, 054002 (2022).
8. D. Mayer, F. Lever, D. Picconi *et al.*, "Following excited-state chemical shifts in molecular ultrafast x-ray photoelectron spectroscopy," Nat. Commun. **13** (2022).
9. X. Wang, R. Y. Engel, I. Vaskivskyi *et al.*, "Ultrafast manipulation of the nio antiferromagnetic order via sub-gap optical excitation," Faraday discussions **237**, 300–316 (2022).
10. V. Chardonnet, M. Hennes, R. Jarrier *et al.*, "Toward ultrafast magnetic depth profiling using time-resolved x-ray resonant magnetic reflectivity," Struct. Dyn. **8**, 034305 (2021).
11. K. Baumgärtner, M. Reuner, C. Metzger *et al.*, "Ultrafast orbital tomography of a pentacene film using time-resolved momentum microscopy at a fel," Nat. Commun. **13**, 2741 (2022).
12. K. Amini, E. Savelyev, F. Brauße *et al.*, "Photodissociation of aligned ch3i and c6h3f2i molecules probed with time-resolved coulomb explosion imaging by site-selective extreme ultraviolet ionization," Struct. Dyn. **5**, 014301 (2018).
13. J. W. L. Lee, D. Tikhonov, P. Chopra *et al.*, "Time-resolved relaxation and fragmentation of polycyclic aromatic hydrocarbons investigated in the ultrafast xuv-ir regime," Nat. Commun. **12**, 6107 (2021).
14. F. Pressacco, D. Sangalli, V. Uhlíř *et al.*, "Subpicosecond metamagnetic phase transition in ferh driven by non-equilibrium electron dynamics," Nat. Commun. **12**, 5088 (2021).
15. F. Roth, M. Borgwardt, L. Wenthaus *et al.*, "Direct observation of charge separation in an organic light harvesting system by femtosecond time-resolved xps," Nat. communications **12**, 1196 (2021).
16. C. Gahl, A. Azima, M. Beye *et al.*, "A femtosecond x-ray/optical cross-correlator," Nat. Photonics **2**, 165–169 (2008).
17. S. Schulz, I. Grguraš, C. Behrens *et al.*, "Femtosecond all-optical synchronization of an x-ray free-electron laser," Nat. Commun. **6**, 5938 (2015).
18. D. E. Rivas, S. Serkez, T. M. Baumann *et al.*, "High-temporal-resolution x-ray spectroscopy with free-electron and optical lasers," Optica **9**, 429–430 (2022).
19. K. Mecseki, H. Höppner, M. Büscher *et al.*, "Hard x-ray induced fast secondary electron cascading processes in solids," Appl. Phys. Lett. **113** (2018).
20. E. Biasin, Z. W. Fox, A. Andersen *et al.*, "Direct observation of coherent femtosecond solvent reorganization coupled to intramolecular electron transfer," Nat. chemistry **13**, 343–349 (2021).
21. E. Allaria, D. Castronovo, P. Cinquegrana *et al.*, "Two-stage seeded soft-x-ray free-electron laser," Nat. Photonics **7**, 913–918 (2013).
22. P. Finetti, H. Höppner, E. Allaria *et al.*, "Pulse duration of seeded free-electron lasers," Phys. Rev. X **7**, 021043 (2017).
23. J. LaRue, B. Liu, G. L. Rodrigues *et al.*, "Symmetry-resolved co desorption and oxidation dynamics on o/ru (0001) probed at the c k-edge by ultrafast x-ray spectroscopy," The J. Chem. Phys. **157** (2022).
24. D. Faccialà, M. Devetta, S. Beauvarlet *et al.*, "Time-resolved chiral x-ray photoelectron spectroscopy with transiently enhanced atomic site selectivity: A free-electron laser investigation of electronically excited fenchone enantiomers," Phys. Rev. X **13**, 011044 (2023).
25. W. Ackermann, G. Asova, V. Ayvazyan *et al.*, "Operation of a free-electron laser from the extreme ultraviolet to the water window," Nat. Photonics **1**, 336–342 (2007).
26. B. Faatz, E. Plönjes, S. Ackermann *et al.*, "Simultaneous operation of two soft x-ray free-electron lasers driven by one linear accelerator," New J. Phys. **18**, 062002 (2016).
27. F. Christie, J. Rönsch-Schulenburg, S. Schreiber *et al.*, "Generation of ultra-short electron bunches and fel pulses and characterization of their longitudinal properties at flash2," WEPAB017, IPAC **17** (2017).
28. R. Ivanov, I. J. B. Macias, J. Liu *et al.*, "Single-shot temporal characterization of xuv pulses with duration from 10 fs to 350 fs at flash," J. Phys. B: At. Mol. Opt. Phys. **53**, 184004 (2020).
29. E. Plönjes, B. Faatz, M. Kuhlmann *et al.*, "Flash2: Operation, beamlines, and photon diagnostics," in *AIP Conference Proceedings,* vol. 1741 (AIP Publishing, 2016).

30. T. Lang, S. Alisauskas, U. Große-Wortmann *et al.*, "Versatile opcpa pump-probe laser system for the flash2 xuv fel beamline at desy," in *The European Conference on Lasers and Electro-Optics,* (Optical Society of America, 2019), p. ca_2_1.
31. A.-L. Viotti, S. Alisauskas, A. Bin Wahid *et al.*, "60 fs, 1030 nm fel pump–probe laser based on a multi-pass post-compressed yb: Yag source," J. synchrotron radiation **28**, 36–43 (2021).
32. J. Ullrich, R. Moshammer, A. Dorn *et al.*, "Recoil-ion and electron momentum spectroscopy: reaction-microscopes," Reports on Prog. Phys. **66**, 1463 (2003).
33. G. Schmid, K. Schnorr, S. Augustin *et al.*, "Reaction microscope endstation at flash2," J. synchrotron radiation **26**, 854–867 (2019).
34. S. Meister, H. Lindenblatt, F. Trost *et al.*, "Atomic, molecular and cluster science with the reaction microscope endstation at flash2," Appl. Sci. **10** (2020).
35. B. Lautenschlager, L. Butkowski, M. Czwalinna *et al.*, "Arrival time stabilization at flash using the bunch arrival corrector cavity (bacca)," in *12th International Particle Accelerator Conference,* (Strahlkontrollen, 2021), PUBDB-2021-04891.
36. A. Angelovski, M. Kuntzsch, M. K. Czwalinna *et al.*, "Evaluation of the cone-shaped pickup performance for low charge sub-10 fs arrival-time measurements at free electron laser facilities," Phys. Rev. Special Top. Beams **18**, 012801 (2015).
37. J. Kim, J. A. Cox, J. Chen *et al.*, "Drift-free femtosecond timing synchronization of remote optical and microwave sources," Nat. Photonics **2**, 733–736 (2008).
38. T. Schibli, J. Kim, O. Kuzucu *et al.*, "Attosecond active synchronization of passively mode-locked lasers by balanced cross correlation," Opt. Lett. **28**, 947–949 (2003).
39. C. Behrens, N. Gerasimova, C. Gerth *et al.*, "Constraints on photon pulse duration from longitudinal electron beam diagnostics at a soft x-ray free-electron laser," Phys. Rev. Special Top. Beams **15**, 030707 (2012).
40. S. Duesterer, M. Rehders, A. Al-Shemmary *et al.*, "Development of experimental techniques for the characterization of ultrashort photon pulses of extreme ultraviolet free-electron lasers," Phys. Rev. Special Top. Beams **17**, 120702 (2014).
41. E. L. Saldin, E. A. Schneidmiller, and M. Yurkov, "Statistical properties of radiation from vuv and x-ray free electron laser," Opt. communications **148**, 383–403 (1998).
42. E. Savelyev, R. Boll, C. Bomme *et al.*, "Jitter-correction for ir/uv-xuv pump-probe experiments at the flash free-electron laser," New J. Phys. **19**, 043009 (2017).
43. M. Krikunova, T. Maltezopoulos, A. Azima *et al.*, "Time-resolved ion spectrometry on xenon with the jitter-compensated soft x-ray pulses of a free-electron laser," New J. Phys. **11**, 123019 (2009).
44. V. Jonauskas, L. Partanen, S. Kučas *et al.*, "Auger cascade satellites following 3d ionization in xenon," J. Phys. B: At. Mol. Opt. Phys. **36**, 4403 (2003).
45. M.Uiberacker, T. Uphues, M.Schultze *et al.*, "Attosecond real-time observation of electron tunnelling in atoms," Nature **446**, 627–632 (2007).
46. D. Rolles, R. Boll, B. Erk *et al.*, "An experimental protocol for femtosecond nir/uv-xuv pump-probe experiments with free-electron lasers," JoVE (Journal Vis. Exp. p. e57055 (2018).
47. I. J. B. Macias, S. Düsterer, R. Ivanov *et al.*, "Study of temporal, spectral, arrival time and energy fluctuations of sase fel pulses," Opt. express **29**, 10491–10508 (2021).
48. A. Ludwig, E. Liberatore, J. Herrmann *et al.*, "Ultrafast relaxation dynamics of the ethylene cation c2h4+," The journal physical chemistry letters **7**, 1901–1906 (2016).